The Astrophysical Journal, 782:9 (11pp), 2014 February 10 doi:10.1088/0004-637X/782/1/9

BLACK HOLE VARIABILITY AND THE STAR FORMATION–ACTIVE GALACTIC NUCLEUS CONNECTION: DO ALL STAR-FORMING GALAXIES HOST AN ACTIVE GALACTIC NUCLEUS?

Ryan C. Hickox[1], James R. Mullaney[2,3], David M. Alexander[3], Chien-Ting J. Chen[1], Francesca M. Civano[1,4], Andy D. Goulding[4], and Kevin N. Hainline[1]
[1] Department of Physics and Astronomy, Dartmouth College, 6127 Wilder Laboratory, Hanover, NH 03755, USA; ryan.c.hickox@dartmouth.edu
[2] Department of Physics & Astronomy, University of Sheffield, Sheffield S3 7RH, UK
[3] Department of Physics, Durham University, South Road, Durham DH1 3LE, UK
[4] Harvard-Smithsonian Center for Astrophysics, 60 Garden Street, Cambridge, MA 02138, USA
Received 2013 June 13; accepted 2013 December 17; published 2014 January 20

ABSTRACT

We investigate the effect of active galactic nucleus (AGN) variability on the observed connection between star formation and black hole accretion in extragalactic surveys. Recent studies have reported relatively weak correlations between observed AGN luminosities and the properties of AGN hosts, which has been interpreted to imply that there is no direct connection between AGN activity and star formation. However, AGNs may be expected to vary significantly on a wide range of timescales (from hours to Myr) that are far shorter than the typical timescale for star formation ($\gtrsim$100 Myr). This variability can have important consequences for observed correlations. We present a simple model in which *all* star-forming galaxies host an AGN when averaged over $\sim$100 Myr timescales, with long-term average AGN accretion rates that are perfectly correlated with the star formation rate (SFR). We show that reasonable prescriptions for AGN variability reproduce the observed weak correlations between SFR and $L_{\rm AGN}$ in typical AGN host galaxies, as well as the general trends in the observed AGN luminosity functions, merger fractions, and measurements of the average AGN luminosity as a function of SFR. These results imply that there may be a tight connection between AGN activity and SFR over galaxy evolution timescales, and that the apparent similarities in rest-frame colors, merger rates, and clustering of AGNs compared to "inactive" galaxies may be due primarily to AGN variability. The results provide motivation for future deep, wide extragalactic surveys that can measure the *distribution* of AGN accretion rates as a function of SFR.

Key words: galaxies: active – galaxies: evolution – quasars: general

Online-only material: color figures

1. INTRODUCTION

There has been a great deal of recent research activity investigating the connection between supermassive black hole (BH) accretion and star formation (SF) in galaxies (for a review see Sections 2 and 3 of Alexander & Hickox 2012). This work is largely motivated by observed correlations between BHs and galaxy properties (e.g., Magorrian et al. 1998; Gebhardt et al. 2000; Ferrarese & Merritt 2000; Gültekin et al. 2009), the remarkable similarity between the global histories of SF and BH accretion (e.g., Boyle & Terlevich 1998; Silverman et al. 2008; Aird et al. 2010; Merloni & Heinz 2013), and the observed tendency of luminous active galactic nuclei (AGNs) to reside in star-forming hosts (e.g., Lutz et al. 2008; Bonfield et al. 2011). Furthermore, a number of theoretical models predict that SF and BH growth should be closely linked in galaxies, driven by a common supply of cold gas (e.g., Di Matteo et al. 2005; Hopkins et al. 2006; Somerville et al. 2008; Hopkins & Quataert 2010; Anglés-Alcázar et al. 2013a) and with energy released by the AGN potentially triggering new SF (e.g., Nayakshin & Zubovas 2012; Zubovas et al. 2013; Nayakshin 2014).

Contrary to these expectations, recent observational studies have found relatively *weak* correlations between BH accretion and SF. While some studies have reported a strong link between SF and AGN activity for high-luminosity AGNs (e.g., Lutz et al. 2008; Bonfield et al. 2011), at lower luminosities these correlations appear relatively weak or absent. Furthermore, typical AGN hosts have star formation rates (SFRs) characteristic of normal star-forming galaxies at a given redshift (e.g., Mullaney et al. 2012b), and moderate-luminosity AGNs exhibit similar SFRs to lower-luminosity sources (e.g., Shao et al. 2010; Rosario et al. 2012; Harrison et al. 2012), suggesting little connection between SF and BH growth in these systems.

Similar conclusions can be drawn from the properties of AGN host galaxies and dark matter halos. Moderate-luminosity AGNs appear to be found in galaxies with a wide range of rest-frame optical or near-IR colors and not simply in blue star-forming galaxies (e.g., Nandra et al. 2007; Georgakakis et al. 2008; Hickox et al. 2009; Silverman et al. 2009; Rosario et al. 2013a; Goulding et al. 2013). AGN host galaxies have colors indistinguishable from those of "normal" galaxies of similar mass and redshift (e.g., Xue et al. 2010; Cardamone et al. 2010; Bongiorno et al. 2012; Hainline et al. 2012; Rosario et al. 2013a), although they do appear to show slightly stronger and more centrally concentrated SF (Santini et al. 2012; Rosario et al. 2013b; LaMassa et al. 2013; Hicks et al. 2013). Likewise, the spatial clustering and thus dark matter halo masses (e.g., Hickox et al. 2009; Coil et al. 2009; Donoso et al. 2010; Li et al. 2006) and morphologies (e.g., Cisternas et al. 2011; Schawinski et al. 2011; Civano et al. 2012; Kocevski et al. 2012) of moderate-luminosity AGNs are generally consistent with those for "normal" galaxies with similar mass, color, and redshift.

These results have frustrated many attempts to uncover the galaxy properties responsible for "triggering" BH activity, leading some authors to conclude that there is little, if any, connection between the growth rate of BHs and SF in their hosts,

at least in moderate-luminosity systems (e.g., Shao et al. 2010). However, other studies have suggested a *strong* correlation between BH growth and SF. The fraction of galaxies with an AGN above a threshold luminosity increases substantially with SFR (e.g., Symeonidis et al. 2011, 2013; Rafferty et al. 2011; Juneau et al. 2013), and the average AGN accretion rate in galaxies scales with stellar mass and redshift in a way that closely mirrors the star-forming "main sequence" (Mullaney et al. 2012a). The average AGN luminosity in interacting pairs of galaxies at low redshift increases with decreasing separation, tracing precisely the behavior that is seen for SF (Ellison et al. 2011, 2013), and Seyfert galaxies show a strong correlation between AGN luminosity and *nuclear* SF (e.g., Diamond-Stanic & Rieke 2012; Esquej et al. 2014). Recently, the connection between galaxy-scale SF and AGN activity was directly tested by Chen et al. (2013), who showed that when star-forming galaxies at $z \sim 0.5$ are divided up by SFR, their average BH accretion rate is directly proportional to their SFR, consistent with previous results for galaxies at higher redshift (Symeonidis et al. 2011; Rafferty et al. 2011).

These observations present the interesting puzzle that the luminosities of individual AGNs show a weak or absent correlation with the properties of their host galaxies, but that BH accretion appears tightly linked to SF in a more global sense (for an extensive review of these results see Alexander & Hickox 2012). In this paper, we explore a possible solution, first suggested by Alexander & Hickox (2012), in which the differences are caused by significant AGN variability on timescales shorter than those characteristic of galaxy evolution (see also Neistein & Netzer 2014 for a detailed discussion of the observational effects of these different timescales). We construct a simple model in which the growth rate of BHs (averaged over galaxy evolution timescales of $\gtrsim$100 Myr) is exactly proportional to the SFR in its host, but the instantaneous *observed* AGN luminosity can vary over a wide dynamic range, and explore the observational consequences of this scenario. In Section 2 we discuss AGN variability, in Section 3 we present the details of the model, in Section 4 we present the implications of this model and compare to observations, and in Section 5 we discuss the results in the context of the cosmological links between BHs and galaxies.

2. AGN VARIABILITY

The process of accretion onto BHs is known to be highly variable with time. Stellar-mass BH binaries exhibit variations in the accretion luminosity on a wide range of timescales, and are observed to change dramatically in luminosity by $\gtrsim$5 orders of magnitude over periods of days to weeks, owing to feedback from the accreting BH and transitions in the mode of accretion (e.g., Chen et al. 1997; Remillard & McClintock 2006). AGNs also show significant but smaller-amplitude (up to two orders of magnitude) variability on timescales from hours to years, observed at optical/UV and X-ray wavelengths that probe accretion disk and coronal emission, respectively (e.g., Ulrich et al. 1997; McHardy 2013). However, this small-scale variability is *not* analogous to accretion state changes in BH binaries, because the dynamical and viscous timescales for accretion increase with BH mass, such that an equivalent state transition that lasts several days in a $10\,M_{\odot}$ binary might be expected to take $\sim 10^4$ yr for a $\sim 10^7\,M_{\odot}$ BH. It is natural to expect that AGNs, like X-ray binaries, experience variability over a large dynamic range in luminosity (Figure 1), corresponding to changes in the accretion state driven by various physical processes including feedback on the accreting material

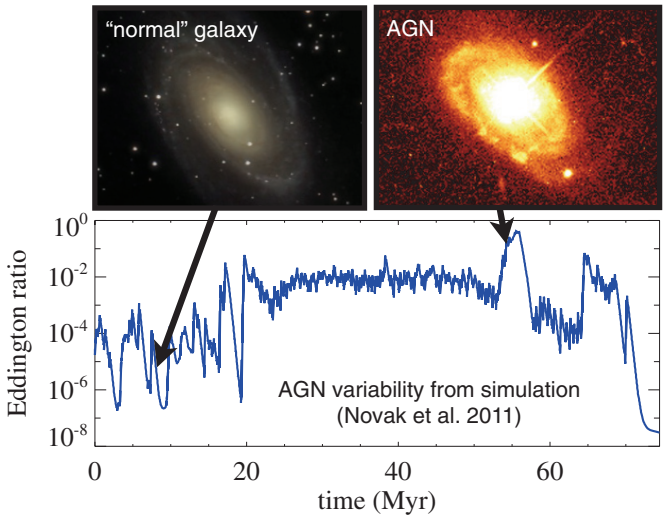

Figure 1. Schematic illustration of AGN variability. The bottom panel shows the Eddington ratio as a function of time for one time interval in a hydrodynamic simulation presented by Novak et al. (2011), shown in the bottom panel of their Figure 6. These simulations suggest that galaxies can switch between an "inactive" state (left panel) and a bright AGN state (right panel) over timescales of ∼Myr or less. Image credits, from left: M81: Wikimedia Commons; PG 0052+251: J. Bahcall (IAS, Princeton), M. Disney (University of Wales), NASA/ESA.

(A color version of this figure is available in the online journal.)

(e.g., Hopkins et al. 2005; Novak et al. 2011) or accretion disk instabilities (e.g., Siemiginowska & Elvis 1997). However, this variability could never be directly observable for an individual AGN over the history of modern astronomy.

There are, however, *indirect* measurements that give us clues to longer-term AGN variability. Recently, AGN light echoes in the form of large [O III]-emitting clouds have been discovered on the outskirts of several galaxies without clear evidence of ongoing AGN activity (Lintott et al. 2009; Schawinski et al. 2010; Keel et al. 2012a, 2012b) or as ultraluminous galaxy-wide narrow-line regions (Schirmer et al. 2013). These large ionized clouds have spectral parameters indicating they were excited by AGN continuum radiation, and the inferred AGN luminosity needed to illuminate these clouds suggests that the source could have been many orders of magnitude (as high as 10^5 times) brighter at a time in the past corresponding to the light-travel time from the nucleus of $\sim 10^4$ yr (Schawinski et al. 2010; Schirmer et al. 2013). Similar evidence comes from the Milky Way, where reflections of X-ray emission off molecular clouds indicate that the Galactic Center varied in brightness by up to $\sim 10^3$ times over the past ∼500 yr (e.g., Ponti et al. 2010; Capelli et al. 2012; Ryu et al. 2013), while the observed "*Fermi* bubbles" observed in γ-ray emission may be relics of an intense AGN phase $\sim 10^6$ yr ago (Zubovas et al. 2011; Zubovas & Nayakshin 2012; Su & Finkbeiner 2012). For luminous quasars at high redshift, the transverse proximity effect provides a measure of the variability based on the sizes of ionized bubbles around the quasars, typically yielding lifetimes for luminous accretion of $\sim 10^6$–10^7 yr (e.g., Jakobsen et al. 2003; Gonçalves et al. 2008; Kirkman & Tytler 2008). For AGNs with relativistic radio-bright jets, observations of hot spots and lobes in the jets, as well as cavities inflated by the mechanical outflows, suggest highly intermittent activity with timescales of $\sim 10^4$–10^7 yr (e.g., McNamara & Nulsen 2007; Siemiginowska et al. 2010). Together, these observations provide clear evidence

that AGN accretion rates can vary by many orders of magnitude on timescales from hundreds to millions of years.

A large dynamic range of variability is consistent with the wide distribution of Eddington ratios observed for AGNs in extragalactic surveys. Studies of nearby optically selected AGNs found that star-forming and passive galaxies have characteristic lognormal and power-law distributions of Eddington ratio that were independent of BH mass (Kauffmann & Heckman 2009). Hopkins & Hernquist (2009) derived Eddington ratio distributions using a range of AGN observations and showed that they can be modeled with a theoretically motivated functional form consisting of a Schechter function, defined as a power law with an exponential cutoff near the Eddington limit:

$$\frac{dt}{d\log L} = t_0 \left(\frac{L}{L_{\rm cut}}\right)^{-\alpha} \exp\left(-L/L_{\rm cut}\right). \quad (1)$$

Hopkins & Hernquist (2009) found that the observed Eddington ratios can be reproduced with $L_{\rm cut} \approx 0.4 L_{\rm Edd}$ and $\alpha \approx 0.6$. This power-law slope is similar to that found by Kauffmann & Heckman (2009) for optically selected AGNs in low-redshift passive galaxies. We note that recent studies suggest that many low-ionization sources included in the low-Eddington optical AGN population are likely to be powered by evolved stellar populations, rather than BH accretion (e.g., Sarzi et al. 2010; Yan & Blanton 2012; Singh et al. 2013), although the effects of this contamination on the derived Eddington ratio distribution are difficult to assess. However, X-ray selected AGNs at moderate to high redshift (which suffer little contamination from sources powered by evolved stars) show a similar universal power-law shape for the specific accretion rate distribution, parameterized by the ratio of $L_{\rm AGN}$ to stellar mass. This distribution is independent of stellar mass, but increases in amplitude with redshift similarly to the evolution of the star-forming "main sequence," suggesting a connection between AGN accretion and SF (Aird et al. 2012; Bongiorno et al. 2012). Aird et al. (2012) obtained a power-law slope to this distribution of $\alpha \approx 0.6$, similar to that measured by Hopkins & Hernquist (2009). Bongiorno et al. (2012) report a somewhat steeper slope ($\alpha \approx 1$), although this is measured over a smaller dynamic range in specific accretion rate. For luminous broad-line quasars, recent studies have directly measured Eddington ratios using the virial technique. Correcting for incompleteness effects, these analyses have yielded similarly broad distributions that cutoff at high Eddington ratios and increase to low accretion rates, although the slopes of these distributions on the low end are less well-constrained than for X-ray selected samples (e.g., Nobuta et al. 2012; Kelly et al. 2010; Kelly & Shen 2013).

For the purposes of the discussion below, we will represent the "observed" AGN luminosity distribution at fixed stellar (or BH) mass using the Hopkins & Hernquist (2009) model given in Equation (1) with $\alpha = 0.6$ and $L_{\rm cut} = 100\langle L_{\rm AGN}\rangle$. This luminosity distribution is shown as the dashed orange line in Figure 2, where $L_{\rm AGN}$ is plotted in terms of its value relative to the long-term average luminosity $\langle L_{\rm AGN}\rangle$. We normalize this distribution (by scaling t_0) such that the integral over all $L_{\rm AGN}$ is equal to 1. The curve therefore represents the *relative* time spent by the AGN in each logarithmic interval of luminosity. This value of $L_{\rm cut}$ adopted here, while somewhat arbitrary, is motivated by two main considerations. First, it reproduces well the observed relationship between SFR and BH accretion rate in powerful AGNs, as shown in Section 4. Second, for a Milky Way type galaxy and our adopted model parameters (as we discuss in Section 3), this value of $L_{\rm cut} \approx 0.4 L_{\rm Edd}$,

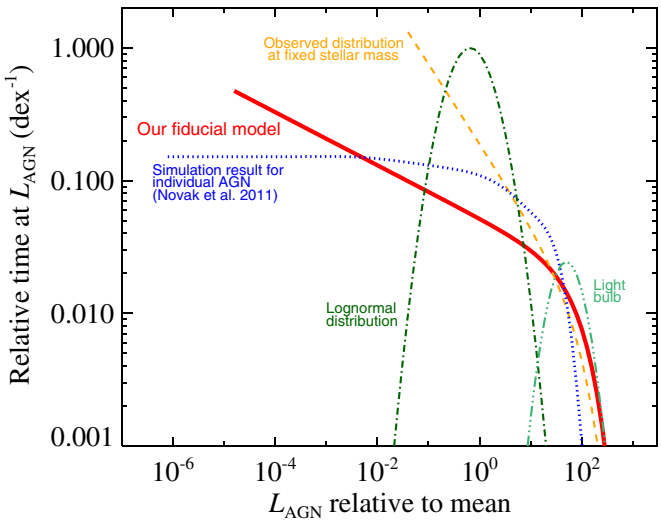

Figure 2. Our fiducial model distribution of AGN luminosity compared to recent observational and theoretical results. The figure shows the relative amount of time spent per logarithmic interval in $L_{\rm AGN}$, plotted in terms of its value relative to the average long-term AGN luminosity. The yellow dashed line shows the Schechter function distribution (Hopkins & Hernquist 2009, Equation (1)) with power-law index $\alpha = 0.6$ that approximately matches observed Eddington ratio and specific accretion rate distributions (Hopkins & Hernquist 2009; Aird et al. 2012; Bongiorno et al. 2012), and consistent with optical spectroscopic studies of AGNs in low-redshift passive galaxies (Kauffmann & Heckman 2009). The green dot-dashed line shows a lognormal distribution, as obtained by Kauffmann & Heckman (2009) for AGNs in low-redshift star-forming galaxies, while the light green dot-dot–dashed line shows a "light bulb" model with a duty cycle $\sim 10^{-2}$ (e.g., Conroy & White 2013). The blue dotted line shows the distribution from the hydrodynamic simulations of Novak et al. (2011), which can be approximately modeled by an exponential (i.e., a Schechter function with $\alpha = 0$). The fiducial model we adopt in this paper consists of Schechter function with $\alpha = 0.2$; this model gives a qualitatively good match to observations of the SF and AGN activity as discussed below. Details of the different distributions are presented in Section 2. We discuss the observational consequences of changing the adopted luminosity distribution in Section 4.4.

(A color version of this figure is available in the online journal.)

consistent with the cutoff adopted by Hopkins & Hernquist (2009) to fit observed Eddington ratio distributions. We note that, by definition, the average luminosity of the distribution equals $\langle L_{\rm AGN}\rangle$, which requires that the distribution be truncated at some lower limit. For $L_{\rm cut} = 100\langle L_{\rm AGN}\rangle$ and $\alpha = 0.6$, we require a lower limit at $L_{\rm AGN} \approx 10^{-2}\langle L_{\rm AGN}\rangle$, as shown in Figure 2. This distribution therefore represents variability of the AGN accretion rate over approximately four orders of magnitude, consistent with the lower limit on the dynamic range observed by a number of studies (e.g., Hopkins & Hernquist 2009; Kauffmann & Heckman 2009; Aird et al. 2012; Bongiorno et al. 2012).

In addition to broad power-law or Schechter function models, several studies have considered narrower distributions for the AGN accretion rate. Kauffmann & Heckman (2009) found that optically selected AGNs in galaxies with young stellar populations show an approximately lognormal distribution in accretion rate (with width $\sigma \approx 0.4$ dex) that is independent of mass. The lognormal distribution is given by

$$\frac{dt}{d\log L} = t_0 \exp\left(-\frac{(\log L - \log L_0)^2}{2\sigma^2}\right) \quad (2)$$

and is shown as the dot–dashed dark green line in Figure 2. We again scale t_0 so that this curve represents the relative time spent in each dex of $L_{\rm AGN}$. The centroid luminosity L_0 depends on σ, to ensure that the average accretion rate in the distribution is

equal to $\langle L_{\rm AGN}\rangle$. For a width $\sigma = 0.4$ dex, $L_0 \approx 0.8\langle L_{\rm AGN}\rangle$, as shown in Figure 2.

A number of works have also considered a "light bulb" scenario in which every galaxy spends a fixed fraction of time "on" as an AGN (with some distribution of accretion rates) and the remainder as a "normal" galaxy at very low Eddington ratio. Employed in a cosmological context, such models can be effective at modeling the quasar luminosity function (LF), clustering, and other observables (e.g., Shankar et al. 2013; Conroy & White 2013), although they do not reproduce observed Eddington ratio distributions for moderate-luminosity AGNs (e.g., Hopkins & Hernquist 2009; Shankar et al. 2013). The recent model of Conroy & White (2013) adopted a lognormal Eddington ratio distribution with $\sigma = 0.3$ dex, for which fits to the quasar LF yielded a duty cycle (the fraction of time the quasar is "on") of $\sim 10^{-3}$–10^{-2} at $z < 3$. In this study we model such a "light bulb" scenario using a lognormal distribution with $\sigma = 0.3$ and $L_0 \approx 50\langle L_{\rm AGN}\rangle$ (chosen to approximately match the SFRs of luminous AGNs, as shown in Section 4.4), with a corresponding duty cycle $\sim 10^{-2}$. In the model, objects in the "off" state are set to an arbitrarily low $L_{\rm AGN} \ll \langle L_{\rm AGN}\rangle$, the precise value of which does not affect the results. This "light bulb" distribution is shown as the light green dot-dot–dashed line in Figure 2.

Several studies have also considered accretion rate distributions that are a sum of power-law and lognormal components. Such a distribution was obtained for the full sample of galaxies (passive and star forming) studied by Kauffmann & Heckman (2009) using optical spectroscopy, and was favored by Shankar et al. (2013) in order to best reproduce Eddington ratio distributions, AGN LF, and other properties of the AGN population across a range of redshifts. The observable quantities (as discussed in Section 4) that are predicted by such combined models are similar to those produced by a pure Schechter function, although the details depend on the relative normalizations of the lognormal and power-law components. For simplicity, we restrict this paper to Schechter and lognormal distributions and do not consider such "combined" models in further detail.

In addition to the observational results discussed above, theoretical understanding of the luminosity distribution of AGNs may be obtained from recent simulations of BH accretion including small-scale feedback (e.g., Hopkins et al. 2005; Ciotti et al. 2010; Novak et al. 2011; Gabor & Bournaud 2013) or a detailed treatment of gravitational torques (e.g., Anglés-Alcázar et al. 2013a, 2013b) that show strong stochastic variations in the BH accretion rate over a range of timescales. The accretion rate distribution from the simulation of Novak et al. (2011) is shown in Figure 2. These simulations shows that the accretion rate for a given BH can vary by more than seven orders of magnitude in a timescale of ∼Myr or less. The model BH spends approximately equal time in any given logarithmic interval of accretion rate, with a cutoff at high accretion rates due to the Eddington limit. This distribution can be approximately described by an exponential (that is, a Schechter function as for the observational results discussed above, but with $\alpha = 0$). Similar results were obtained in recent simulations by Gabor & Bournaud (2013), who found that the characteristic power-law slope of the accretion rate distribution varies depending on gas fraction, from $\alpha \approx 0.6$ for a galaxy like the Milky Way to $\alpha \approx 0.2$ for systems with a higher gas fraction characteristic of galaxies at $z = 2$.

On the whole, Figure 2 illustrates the wide diversity in AGN accretion rate and luminosity distributions that are obtained from theoretical models and observational studies of different galaxy populations. For most of what follows we will adopt a fiducial distribution that lies between the Novak et al. (2011) theoretical and Hopkins & Hernquist (2009) observational curves, following the Schechter functional form in Equation (1), with $\alpha = 0.2$ and $L_{\rm cut} = 100\langle L_{\rm AGN}\rangle$. As shown in Figure 2, this distribution requires a lower limit to $L_{\rm AGN}$ of $\sim 10^{-5}\langle L_{\rm AGN}\rangle$. We note that the precise value of $L_{\rm cut}$ makes no significant difference to our results; increasing or decreasing $L_{\rm cut}$ by a factor of two changes the model predictions by less than the observational uncertainties on the various quantities discussed in Section 4.

As we demonstrate in Section 4, our fiducial distribution displays a good qualitative agreement with a range of observational data. However, we stress that in this study we do *not* attempt to constrain the precise distribution in AGN luminosity or estimate uncertainties. Such an analysis would require a very careful understanding of the biases and uncertainties in the various observational constraints and will likely suffer from significant degeneracies in the functional form for the distribution in $L_{\rm AGN}$. Rather, the scope of this work is limited to showing that with a reasonable choice of the luminosity distribution, short-term variability of the AGN can explain a range of observations even if BH accretion and SF are perfectly correlated on timescales typical of galaxy evolution. We describe this simple model in the next section.

3. A SIMPLE MODEL CONNECTING BLACK HOLE ACCRETION AND STAR FORMATION

Motivated by our knowledge of AGN variability and the observed and theoretical links between SF and BH accretion, we may ask a straightforward question: Observed over timescales typical of SF ($\gtrsim$100 Myr; e.g., Hickox et al. 2012) do *all* star-forming galaxies host an AGN? Here we construct a simple model in which SF and (long term) BH growth are perfectly correlated in galaxies, and explore the observational consequences. The ingredients of the model are as follows.

1. We create a model population of star-forming galaxies across a range of redshifts from 0 to 2, with a redshift-dependent distribution in SFR taken from the far-IR LF derived by Gruppioni et al. (2013) from *Herschel* observations. We convert far-IR luminosity to SFR using the prescription of Kennicutt (1998), multiplying by a factor of 0.6 as appropriate for a Chabrier (2003) initial mass function (IMF). We include galaxies with total far-IR luminosities $10^9 < L_{\rm IR} < 10^{14}\ L_\odot$, covering the full luminosity range that is well constrained by the *Herschel* LF measurements at any redshift (Gruppioni et al. 2013) and corresponding to SFRs characteristic of essentially all star-forming galaxies ($\sim$0.1–$10^4\ M_\odot\ {\rm yr}^{-1}$). Varying these limits in $L_{\rm IR}$ by an order of magnitude has no effect on our conclusions.
2. For each galaxy, we assign an *average* BH accretion rate (i.e., averaged over $\gtrsim$100 Myr) such that SFR/BHAR = 3000, motivated by the observed ratios of SF and BH accretion rates (Rafferty et al. 2011; Mullaney et al. 2012a; Chen et al. 2013).
3. For each galaxy, we assume that the *instantaneous* accretion rate relative to the average is drawn from the fiducial luminosity distribution shown in Figure 2. We note that the adopted distribution is in *luminosities* rather than Eddington ratios, because for simplicity we do not account for the BH mass in each model galaxy. We also stress that the particular timescales over which these variations occur (and thus the

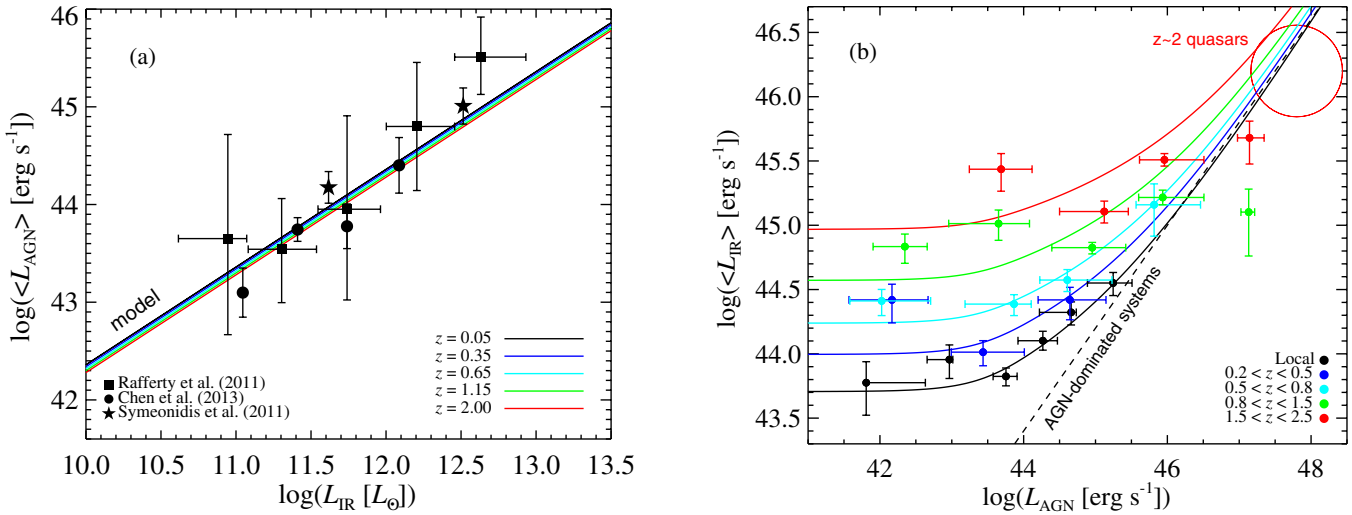

Figure 3. Comparison of the predictions of our AGN variability model to observations of SF and AGN activity in galaxies. (a) The average AGN luminosity for star-forming galaxies as a function of the observed $L_{\rm IR}$. The model predictions for each redshift are shown by the colored lines. By design, these show a constant one-to-one correlation between $\langle L_{\rm AGN}\rangle$ and $L_{\rm IR}$ at all redshifts (the lines are offset for clarity), independent of the choice of accretion rate distribution. The points show recent observational results, which are consistent with this simple picture. (b) The average $L_{\rm IR}$ for AGN host galaxies, as a function of $L_{\rm AGN}$. Data points are taken from Rosario et al. (2012), and solid lines show the predictions of our fiducial model. The models curves are evaluated at the central redshift of each range; the "local" model which is calculated for $z = 0.05$, the median redshift for the *Swift* Burst Alert Telescope AGNs used in the analysis (Rosario et al. 2012; Cusumano et al. 2010). The red circle shows the approximate range of $L_{\rm IR}$ observed for quasars at $z \sim 2$ (Lutz et al. 2008) and the dashed line shows the approximate relation between AGN and IR luminosity for AGN-dominated systems ($L_{\rm IR} \propto L_{\rm AGN}^{0.8}$) determined by Netzer (2009). Our simple model clearly reproduces the general trends in the Rosario et al. (2012) data while also matching the close relation between $L_{\rm AGN}$ and $L_{\rm IR}$ for AGN-dominated systems (Lutz et al. 2008; Netzer 2009).

(A color version of this figure is available in the online journal.)

precise variability power spectrum) are not important in this model. We require only that the fluctuations occur on timescales significantly shorter than a typical SF timescale of $\gtrsim$100 Myr, so that the distribution of AGN luminosities is well sampled at any given SFR.

4. We convert the instantaneous accretion rate $\dot{m}_{\rm BH}$ to a bolometric AGN luminosity via $L_{\rm AGN} = \epsilon \dot{m}_{\rm BH} c^2$, assuming a constant radiative efficiency $\epsilon = 0.1$.[5]

This procedure yields a model population of AGNs and galaxies with an instantaneous BH accretion rate (given by $L_{\rm AGN}$) and SFR (given by $L_{\rm IR}$) that can be compared to observations. With this simulated population of galaxies and AGNs in hand, we can then calculate the same relationships between SF and AGN luminosity that have been derived from recent extragalactic surveys.

4. RESULTS

4.1. Star Formation Rate and L_{AGN}

We begin by calculating the average AGN luminosity for galaxies in bins of $L_{\rm IR}$ for a range of redshifts from 0 to 2. This process serves to average over the variability of the AGNs for a given SFR, and so by the design of the model, produces an exactly proportional relationship between $L_{\rm IR}$ and $\langle L_{\rm AGN}\rangle$ that is independent of redshift, as shown in Figure 3(a). This relationship agrees with that observed in the recent studies of the average BH accretion rate in star-forming galaxies (Symeonidis et al. 2011; Rafferty et al. 2011; Chen et al. 2013). For the Symeonidis et al. (2011) result we have computed the $\langle L_{\rm AGN}\rangle$ in bins of $L_{\rm IR}$ from the data points reported in their paper, as discussed in Chen et al. (2013).

We next perform the opposite calculation, and compute the average $L_{\rm IR}$ as a function of $L_{\rm AGN}$. In the context of our model, this entails selecting galaxies based on the *unstable*, rapidly varying quantity (BH accretion rate or $L_{\rm AGN}$) and averaging over the *stable* quantity (SFR or $L_{\rm IR}$). This analysis is motivated by several recent measurements that have found weak correlations between average SF luminosity and $L_{\rm AGN}$ (Lutz et al. 2010; Shao et al. 2010; Rosario et al. 2012; Harrison et al. 2012). The observed data points from Rosario et al. (2012) are shown in Figure 3(b), converting from νL_ν at 60 μm (as presented in their work) to $L_{\rm IR}$ (integrated from 8–1000 μm) by adding 0.2 dex, as is typical for the average spectral energy distributions of star-forming galaxies (Chary & Elbaz 2001; Kirkpatrick et al. 2013). We also show the observed relationships for optically selected AGN-dominated systems (Netzer 2009) and for high-redshift quasars (Lutz et al. 2008).

To compare our simple model to these results, we select our simulated AGNs in bins of their observed (instantaneous) $L_{\rm AGN}$, and then average the $L_{\rm IR}$ for the objects in each bin. The model results are shown as solid lines in Figure 3(b), and closely match the key features of the observations. In particular, there is no strong correlation between $\langle L_{\rm IR}\rangle$ and $L_{\rm AGN}$ for moderate-luminosity AGN, with each luminosity having an average $L_{\rm IR}$ corresponding to the typical SFR (the "knee" of the IR LF) at each redshift. This average correspondingly shifts to higher luminosity with redshift as the typical SFR of galaxies increases (e.g., Noeske et al. 2007; Elbaz et al. 2011). Figure 4 shows the predicted distribution of $L_{\rm IR}$ for various $L_{\rm AGN}$ and redshift, demonstrating this shift to higher $L_{\rm IR}$ for increasing z.

Another important feature of the model is the emergence of a correlation between $\langle L_{\rm IR}\rangle$ and $L_{\rm AGN}$ at high luminosity. In the model, the highest AGN luminosities can only be produced by galaxies with high SFRs that are near the high end of

[5] Assuming $\epsilon = 0.1$ and SFR/BHAR = 3000, a Milky Way type galaxy with SFR = 1 $M_\odot$ yr^{-1} (e.g., Robitaille & Whitney 2010) will have $\langle L_{\rm AGN}\rangle \approx 2 \times 10^{42}$ erg s^{-1}. The Eddington limit for a 4×10^6 $M_\odot$ BH (Ghez et al. 2008; Gillessen et al. 2009) is $L_{\rm Edd} \approx 5 \times 10^{44}$ erg s^{-1}, so that for $L_{\rm cut} = 100$ $\langle L_{\rm AGN}\rangle$, $L_{\rm cut} \approx 0.4 L_{\rm Edd}$ for the Milky Way as discussed in Section 2.

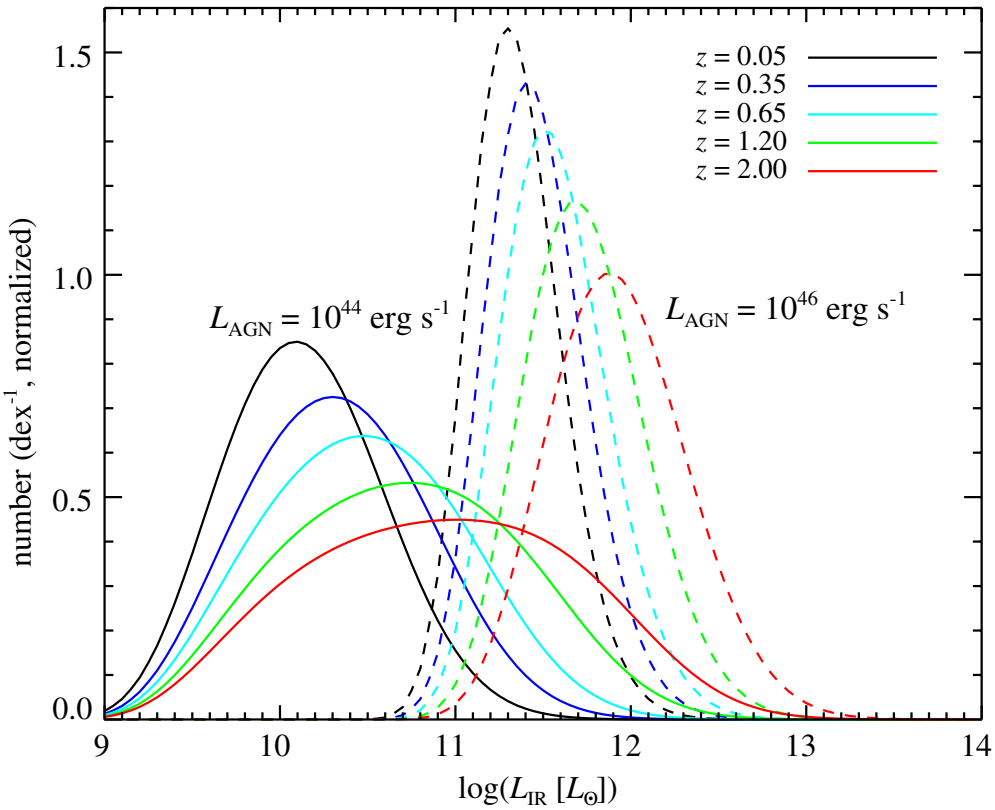

Figure 4. Distributions of L_{IR} predicted by our simple model for AGNs with moderate $L_{AGN} = 10^{44}$ erg s^{-1} (solid lines) and high $L_{AGN} = 10^{46}$ erg s^{-1} (dashed lines), evaluated at the same redshifts (coded by color) as in Figure 3. The distributions are normalized so that the integral under each curve is equal to 1. This figure demonstrates two key aspects of our model for the connection between SF and AGN activity: a shift to higher L_{IR} with increasing redshift at fixed L_{AGN}, and the narrow distribution of L_{IR} for high-luminosity AGNs compared to systems with lower L_{AGN}.

(A color version of this figure is available in the online journal.)

the accretion rate distribution, so that high-luminosity AGNs are associated with narrower distributions in L_{IR} than lower-luminosity AGNs (as shown in Figure 4). Thus there emerges a strong correlation between $\langle L_{IR}\rangle$ and L_{AGN}, as observed in a number of studies (e.g., Lutz et al. 2008; Netzer 2009; Bonfield et al. 2011). We note that this correlation is not due to contamination of the IR emission by the nucleus, as the AGN contribution at far-IR wavelengths is minimal (Netzer et al. 2007; Mullaney et al. 2011; Rosario et al. 2012). In the model, the luminosity at which we begin to see a strong correlation between L_{IR} and L_{AGN} increases with redshift as the "knee" of the IR LF shifts to higher luminosities, explaining the fact that the weak correlations between $\langle L_{IR}\rangle$ and L_{AGN} extend to higher L_{AGN} in the observations at higher z.

Overall, this simple model produces remarkable agreement with both the results on the average AGN luminosity of SF galaxies (Symeonidis et al. 2011; Rafferty et al. 2011; Chen et al. 2013) and the average SFR of AGNs (Lutz et al. 2010; Shao et al. 2010; Rosario et al. 2012). We conclude that the current observations are consistent with a picture in which SF and BH accretion are closely connected over long timescales, but this correlation is hidden at low to moderate L_{AGN} due to the short-term AGN variability.

4.2. The AGN Luminosity Function

As a further check on our simple prescription, we determine the LF of AGNs in our model and compare to observations. A number of previous studies have used the observed AGN LF to place constraints on the BH accretion rate distribution (e.g., Siemiginowska & Elvis 1997; Hopkins et al. 2005; Merloni & Heinz 2008; Shen & Kelly 2012; Conroy & White 2013). In our model, we produce a predicted AGN LF by scaling the observed IR LF from Gruppioni et al. (2013) to the expected AGN luminosities assuming no variability, applying the appropriate factors to convert from L_{IR} to SFR and then to L_{AGN}, via

$$\langle L_{AGN}\rangle = \left(\frac{L_{IR}}{C_{IR}}\right)\left(\frac{1}{3000}\right)\epsilon c^2, \quad (3)$$

where C_{IR} is the L_{IR} to SFR conversion factor from Kennicutt (1998) assuming a Chabrier IMF, and the radiative efficiency $\epsilon = 0.1$ as discussed above. We then convolve the distribution in $\langle L_{AGN}\rangle$ with our adopted distribution in accretion rates, to obtain the predicted "observed" distribution in L_{AGN}. We compare to the bolometric AGN LF determined by Hopkins et al. (2007).

The observed AGN LF along with the model distributions in $\langle L_{AGN}\rangle$ and "observed" L_{AGN} are shown in Figure 5, for four different redshifts. Approximate uncertainties on $\phi(L_{AGN})$ from Hopkins et al. (2007) are shown by the gray shaded region. The model reproduces the general shape and redshift evolution of the AGN LF remarkably well, particularly around the "knee" where the LF is best constrained. We note that at all redshifts the model slightly underpredicts the observed LF, but this may be expected; as we discuss in Section 5, clustering and population studies indicate a non-negligible fraction of AGNs residing in passive galaxies that would not be accounted for in a model that ties all accretion to SF.

Nonetheless, our model may explain why the AGN LF shows a broader high-luminosity tail compared to IR LF. In the model,

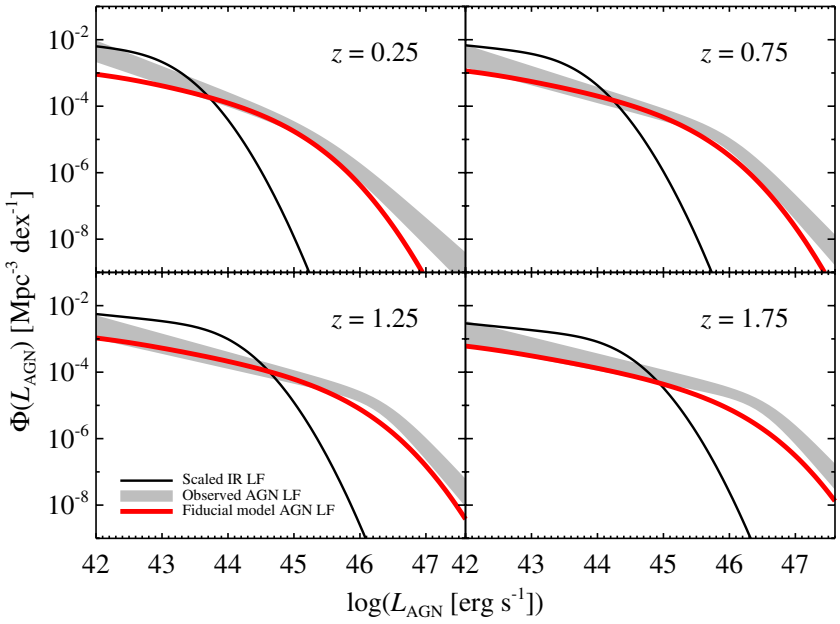

Figure 5. Predictions of our simple model for the AGN luminosity function. Black lines show the distribution in *average* AGN luminosity, determined by scaling the observed IR LF (Gruppioni et al. 2013) to the corresponding $L_{\rm AGN}$ as described in Section 4.2. The red lines show the predicted AGN LF from our fiducial variability model, derived by convolving the average AGN LF with the luminosity distribution shown in Figure 2. The shape and evolution of the LF predicted by the model agrees well with the observed AGN bolometric LF determined by Hopkins et al. (2007), as shown by the gray shaded region. We use the fitting formula from Hopkins et al. (2007) for the "full" redshift evolution of $\phi(L_{\rm AGN})$, and estimate the uncertainties on the LF parameters based on typical uncertainties in fits to individual redshift ranges, given in Table 2 of Hopkins et al. (2007). This result clearly shows that the differences between the characteristic shapes of the IR and AGN LFs can be largely explained by AGN variability.

(A color version of this figure is available in the online journal.)

each galaxy with a high SFR can have a fairly wide range of $L_{\rm AGN}$, which serves to flatten the luminosity distribution and extend it to higher luminosities. The observed AGN LF is thus broadly consistent with the view that AGN activity is ubiquitous in star-forming galaxies and directly follows SF over long timescales, but with significant stochastic variability.

4.3. Merger Fractions

Another interesting test of our simple picture is a comparison to the fraction of AGNs observed in galaxy mergers. A number of theoretical models predict that AGN fueling is primarily driven by mergers (e.g., Hopkins et al. 2006; Somerville et al. 2008), and some recent studies have found enhanced evidence for mergers and interactions in typical low-redshift AGNs (e.g., Koss et al. 2010; Sabater et al. 2013). However, a number of other studies of higher-redshift sources have found that the hosts of typical moderate-luminosity AGNs are no more likely than comparable "normal" galaxies to show morphological disturbances characteristic of mergers (e.g., Cisternas et al. 2011; Schawinski et al. 2011; Civano et al. 2012; Kocevski et al. 2012), with little dependence on the merger fraction $f_{\rm merge}$ with observed $L_{\rm AGN}$ (Kocevski et al. 2012). Other results have suggested that $f_{\rm merge}$ increases at very high $L_{\rm AGN}$ (e.g., Urrutia et al. 2008) leading to the conclusion that BH growth can be triggered by major interactions, but only at the highest luminosities (Schawinski et al. 2012; Treister et al. 2012).

In contrast to AGNs, star-forming galaxies consistently show a significant increase in the merger fraction across a wide range $L_{\rm IR}$ (e.g., Shi et al. 2009; Kartaltepe et al. 2010, 2012), suggesting that more rapidly star-forming galaxies are increasingly more likely to be associated with mergers (keeping in mind that being *associated* with mergers does not necessarily imply merger *triggering*; Hopkins et al. 2010). Adopting the assumptions of our simple model, we can calculate the fraction of AGNs in mergers as a function of observed $L_{\rm AGN}$ for a scenario in which the merger fraction increases with SFR, and thus the time-averaged BH growth rate. We adopt the relationship between $f_{\rm merge}$ and $L_{\rm IR}$ obtained using deep *Hubble Space Telescope* rest-frame optical imaging of luminous star-forming galaxies (Kartaltepe et al. 2012). Here we use the fractions shown in Figure 9 of Kartaltepe et al. (2012), for two different merger classifications. Over the range $11 < \log(L_{\rm IR}\ [L_\odot]) < 12.5$, the value of $f_{\rm merge}$ for "mergers and interactions" increases from $\approx$0.3 to $\approx$0.6, while for "mergers, interactions, and irregulars" (which may include some minor mergers), $f_{\rm merge}$ goes from $\approx$0.4 to $\approx$0.9. We linearly extrapolate these fractions to higher and lower $\log L_{\rm IR}$ (keeping the minimum and maximum fractions to 0 and 1), and assume that this relation between $f_{\rm merge}$ and $L_{\rm IR}$ is constant with redshift. This assumption is motivated by observations showing that the merger fraction for luminous IR galaxies is similar in the local universe (e.g., Wang et al. 2006; Ellison et al. 2013) to that at higher redshifts (e.g., Melbourne et al. 2005; Hung et al. 2013), as well as studies that directly measure merger fractions with a full accounting for redshift effects, showing little evidence for variation with redshift (Shi et al. 2009; Kartaltepe et al. 2012). To obtain predictions for $f_{\rm merge}$ from our model, we determine a merger probability for each of our model galaxies based on its $L_{\rm IR}$ and the corresponding $f_{\rm merge}$ from Kartaltepe et al. (2012). We then select model galaxies in bins of (instantaneous) $L_{\rm AGN}$ and calculate the total $f_{\rm merge}$ by averaging the merger probability for all objects in that bin.

The model predictions are shown in Figure 6, compared to observational data compiled by Treister et al. (2012) and typical merger fractions for control samples of inactive galaxies (Cisternas et al. 2011; Kocevski et al. 2012). We note that these

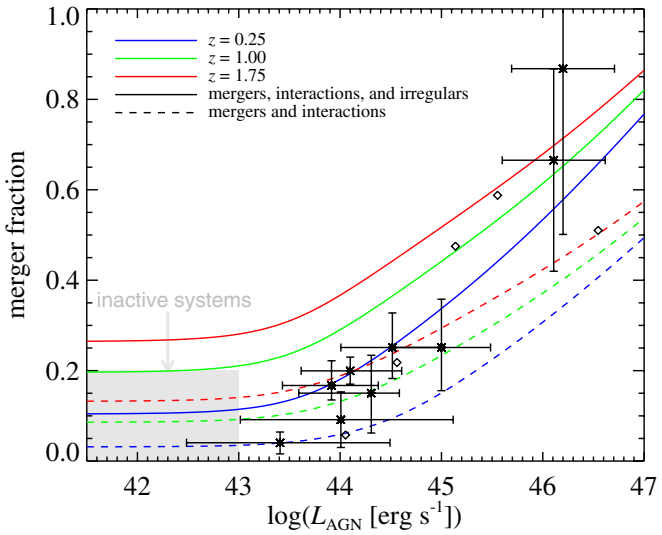

Figure 6. Predictions of our fiducial model on the fraction of AGNs in mergers as a function of AGN luminosity. Data points are taken from the compilation of Treister et al. (2012), and the gray shaded area indicates the typical range of merger fractions for inactive galaxies in the control samples studied by Cisternas et al. (2011) and Kocevski et al. (2012). The colored curves show the predictions of our model assuming a correlation between merger fraction and $L_{\rm IR}$ determined by Kartaltepe et al. (2012). The models are evaluated using the relationships from Kartaltepe et al. (2012) for "mergers, interactions, and irregulars" (solid lines) and "mergers and interactions" (dashed lines). The colors represent the model predictions for different redshifts. The model predicts a weak correlation between $f_{\rm merge}$ and $L_{\rm AGN}$ at low luminosities, with a stronger correlation emerging for the highest-luminosity systems, matching the general trends in the observational data.

(A color version of this figure is available in the online journal.)

observed AGN merger fractions are obtained using a variety of different methods, such as detailed morphological analysis and counts of close companions, which complicates the comparison between individual data points (for a discussion see Section 1 of Kartaltepe et al. 2012). A clear trend is nonetheless evident in the data, showing a weak dependence of $f_{\rm merge}$ on $L_{\rm AGN}$ at low luminosity, with a strong upturn at high $L_{\rm AGN}$. The models clearly reproduce this trend, owing to the fact that in our simple model, luminous AGNs are always associated with rapidly star-forming galaxies while less luminous AGNs are drawn from a mix of galaxy populations. The weak dependence of the merger fraction on AGN luminosity at low $L_{\rm AGN}$ may explain the observations that at moderate to high redshift, moderate-luminosity AGNs have indistinguishable merger fractions from normal galaxies (Cisternas et al. 2011; Schawinski et al. 2011; Kocevski et al. 2012). As is clear from Figure 6, the merger fractions predicted by the model depend on the choice of merger classification adopted from Kartaltepe et al. (2012); the inclusion of irregular systems naturally produces a higher $f_{\rm merge}$ at all $L_{\rm IR}$. However despite these differences, the general trends in the relationship between $f_{\rm merge}$ and $L_{\rm AGN}$ are identical in the two cases, and match those seen in the observational results.

Based on the assumptions of our simple model, we can determine the fraction of the total BH growth that is associated with mergers at different redshifts. We use the curves of $f_{\rm merge}(L_{\rm AGN})$ shown in Figure 6 and the bolometric AGN LF determined by Hopkins et al. (2007). Assuming a constant radiative efficiency (as we have done throughout) such that the accretion rate $\dot{m}_{\rm BH} \propto L_{\rm AGN}$, we compute the average $f_{\rm merge}$ for AGN weighted by the distribution in AGN growth rates, given by $L_{\rm AGN}\phi(L_{\rm AGN})$. This yields a "total" merger fraction of 23% at $z = 0$, rising to 72% at $z = 2$, for our model including irregular systems (these fractions are 10% and 44%, respectively, if we assume the fractions for only "mergers and interactions"). These results are consistent with a picture in which mergers are an important driver for global BH growth at high redshift, with secular processes becoming increasingly dominant at low redshift (e.g., Draper & Ballantyne 2012).

4.4. Effect of Changing the Accretion Rate Distribution

The previous analyses have focused on the predictions of our simple model including our "fiducial" distribution of AGN accretion rates (and equivalently, luminosities). We stress that while the shape of our fiducial distribution is characteristic of those obtained from recent theoretical and observational studies (as discussed in Section 2), it is not obtained by a formal fit to the data. Here we explore the implications of other distributions in the accretion rate, focusing on the recent measurements and theoretical results illustrated in Figure 2.

We first note that, by design, all the models predict the simple linear relation between $\langle L_{\rm AGN}\rangle$ and $L_{\rm IR}$ shown in Figure 3(a), independent of redshift and the choice of accretion rate distribution. In contrast, the models produce significant differences in the inverse relationship, between observed $L_{\rm AGN}$ and $\langle L_{\rm IR}\rangle$, as discussed in Section 4.1. The model predictions for the different luminosity distributions are shown in Figure 7(a), along with the observational data from Rosario et al. (2012). The general trends in the data are reproduced by all the models with low-luminosity power-law distributions and a large dynamic range in accretion rate. These all show a weak correlation between $L_{\rm AGN}$ and $\langle L_{\rm IR}\rangle$ at moderate $L_{\rm AGN}$, with a stronger correlation at high luminosity. The observed distribution at fixed mass (with $\alpha = 0.6$) further shows strong correlation at low $L_{\rm AGN}$, due to the fact that the distribution is forced to cut off at a relatively high average luminosity to avoid diverging (Figure 2), so that very low-luminosity AGN are at the very bottom end of the accretion rate distribution. In contrast to the results for distributions with a wide dynamic range, a relatively tight lognormal distribution in accretion rates (either in the lognormal or "light bulb" cases) yields a strong correlation between $L_{\rm AGN}$ and $\langle L_{\rm IR}\rangle$ at all $L_{\rm AGN}$, in conflict with the observations. We note that the "light bulb" model reproduces well the strong correlation between $L_{\rm AGN}$ and $\langle L_{\rm IR}\rangle$ at high luminosities, but does not produce the observed weak correlation at moderate to low $L_{\rm AGN}$. This figure demonstrates that models in which AGN experience a broad dynamic range in accretion rate (and luminosity) can fit the general observed trends, and that our fiducial distribution can reproduce the observations particularly well.

We next focus on the predicted AGN LFs, as discussed in Section 4.2. The model predictions for the different luminosity distributions are shown in Figure 7(b). Again, we find that all the models with broad power-law luminosity distributions can reproduce the general trends in the observed AGN LF, although they do not produce enough AGNs at the very highest luminosities. (This may be evidence for a somewhat flatter tail in the accretion rate distribution than is modeled by a Schechter function; e.g., Aird et al. 2013.) In contrast, the lognormal distribution strongly underpredicts the number of AGNs at moderate to high luminosities, since the AGN luminosity is fairly tightly tied to $L_{\rm IR}$. Interestingly, the "light bulb" model results in a similar LF to that predicted by our fiducial model on the high-luminosity end, although it produces fewer low-luminosity AGNs. This general agreement with the observed AGN LF has been found by previous studies of "light bulb"

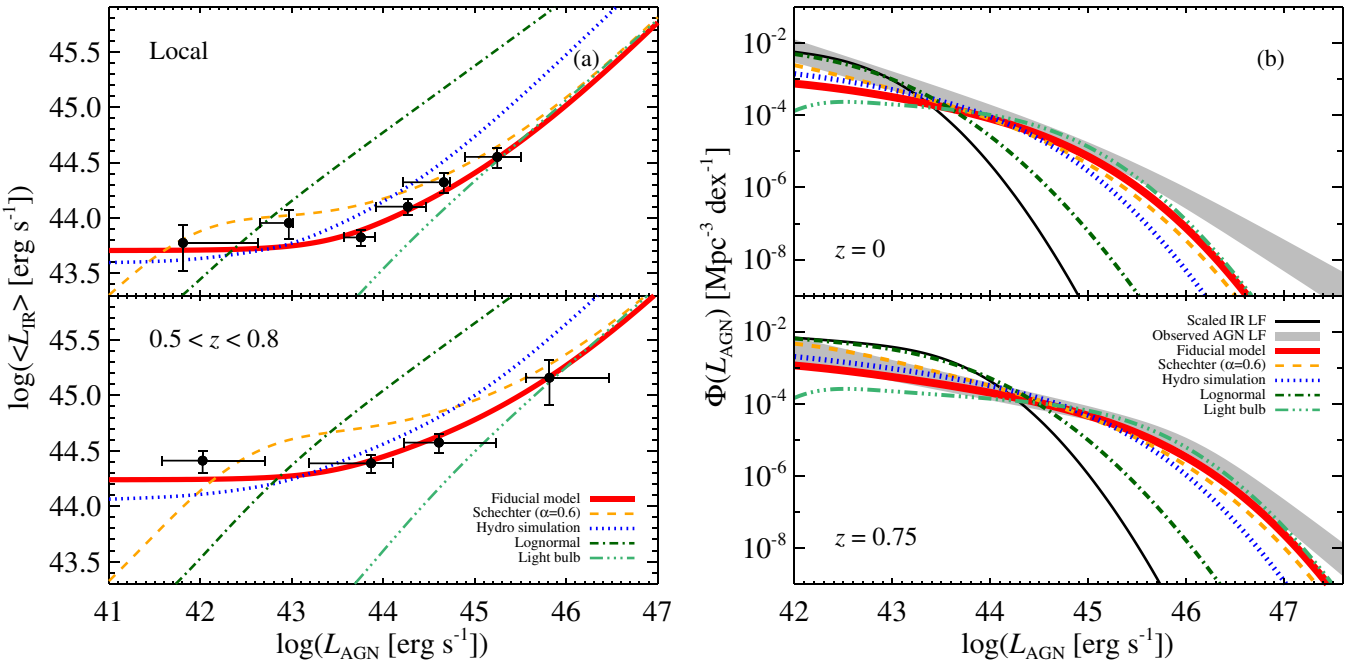

Figure 7. Comparison of the predictions of different AGN luminosity distributions for (left) the average SFR as a function of $L_{\rm AGN}$, as in Figure 3(b), and (right) the AGN LF, as in Figure 5, for two representative redshift ranges. Both the distribution obtained by the Novak et al. (2011) simulation (blue dotted line) and our fiducial model (red solid line) can broadly reproduce both the observed trends with SF and the AGN LF. The steep observed AGN luminosity distribution at fixed stellar or BH mass (Hopkins & Hernquist 2009; Aird et al. 2012, modeled by the Schechter function with $\alpha = 0.6$) also produces a weak trend in the $\langle$SFR$\rangle$ versus $L_{\rm AGN}$ (although less closely matching the data) and fits the AGN LF particularly well. In our simple picture, a "lognormal" luminosity distribution (Kauffmann & Heckman 2009) yields too strong a correlation between $\langle$SFR$\rangle$ and $L_{\rm AGN}$ and fails to produce the high-luminosity tail of the AGN LF.

(A color version of this figure is available in the online journal.)

models where the accretion rates are scaled to BH or galaxy mass rather than SFR (e.g., Siemiginowska & Elvis 1997; Conroy & White 2013). We conclude that, in the context of our AGN variability model, reproducing the general trends in the observed AGN LF requires that the AGN luminosity distribution must extend to relatively high $L_{\rm AGN}$ above the long-term average luminosity. However, predictions for the AGN LF are relatively insensitive to the precise choice of luminosity distribution, indicating that the relationship between $\langle L_{\rm IR}\rangle$ and $L_{\rm AGN}$ may provide a better constraint on the nature of the AGN variability.

5. DISCUSSION

We have shown that the observed relationships between AGN luminosity, SF, and galaxy mergers, as well as the relative shapes of the IR and AGN LFs, can be broadly explained by a simple picture in which BH accretion rates are perfectly connected to SFRs, but subject to short-timescale variability over a large dynamic range. This picture may have significant implications for studies of AGN triggering, as it implies that the observed *instantaneous* luminosity of an AGN is a weak indicator of the *average* BH accretion rate on the timescales of the galaxy evolution processes that may be expected to drive the long-term growth of BHs. Thus powerful quasars may represent brief upward fluctuations in the AGN luminosity of otherwise passive systems, while seemingly "normal" galaxies may have experienced powerful AGN activity and rapid BH growth in the recent past.

AGN feedback is not explicitly included in this analysis; however the strong correlation between SFR and long-term BH accretion rate prescribed by our model may suggest indirectly that some feedback processes are occurring. Small-scale feedback, in which the energy released by the BH limits its own gas supply, is consistent with our model as it is the key physical process that drives rapid variability of the AGN over a large dynamic range in a number of theoretical studies (e.g., Hopkins et al. 2005; Ciotti et al. 2010; Novak et al. 2011; Gabor & Bournaud 2013). On larger scales, a particularly tight connection between SFR and BH accretion is predicted by some models of positive feedback in which AGN activity triggers SF (e.g., Zubovas et al. 2013; Nayakshin 2014), but such a correlation over long timescales can arise in models with zero or even negative AGN feedback (e.g., Anglés-Alcázar et al. 2013a; Gabor & Bournaud 2013), so these results alone do not enable us to draw any strong conclusions about the effects of BH feedback on galaxy-wide SF.

Indeed, despite its remarkable success in reproducing a range of observational results, our model is too simplistic to yield information on the details of AGN fueling and variability. For example, our model assumes a perfect proportionality between SFR and long-term BH accretion rate and does not allow for any scatter in this relationship. Relatively small scatter in the BHAR/SFR ratio would be equivalent to simply broadening the observed AGN luminosity distribution at a fixed SFR, although large intrinsic scatter in this ratio would flatten the observed correlation between $\langle L_{\rm AGN}\rangle$ and $L_{\rm IR}$ shown in Figure 3(a), and so would be inconsistent with observations (for a discussion see Chen et al. 2013). While the strong observed correlation suggests that the intrinsic scatter in the BHAR/SFR ratio is relatively small, this scatter must be constrained independently in order to extract the true variability in AGN luminosities.

Another limitation of our model is that, in order to keep it as simple as possible, we do not include any consideration of galaxy or BH masses. We therefore explicitly ignore the dependence of the Eddington limit on BH mass. This may

thus cause us to overpredict the number of luminous AGNs in small but rapidly star-forming galaxies with small BHs, and underpredict the maximum luminosities of massive galaxies with large BHs. Indeed, the tendency of AGNs to be found in relatively massive galaxies (e.g., Kauffmann et al. 2003; Colbert et al. 2005; Haggard et al. 2010; Xue et al. 2010; Cardamone et al. 2010) and halos (e.g., Hickox et al. 2009, 2011; Coil et al. 2009; Starikova et al. 2011; Allevato et al. 2011; Cappelluti et al. 2012), and the corresponding existence of relatively powerful AGNs in massive but passive systems (as discussed in Section 4.2) are likely a direct consequence of the Eddington limit (e.g., Hopkins et al. 2009; Aird et al. 2012). In the context of our model, introducing an Eddington limit would be equivalent to varying the luminosity at which the distributions cut off on the high end, depending on the relationship between SFR and BH mass in each galaxy.

A more sophisticated version of our model would therefore account for the joint distribution of BH (and galaxy) masses and SFRs, while including an explicit Eddington limit. This could be achieved analytically by a similar process to that described here, but expanded to include a careful treatment of the observed redshift evolution in the galaxy stellar mass and LFs (similar to the analysis of Conroy & White 2013) while also accounting for the distribution of SFRs as a function of galaxy mass, as in recent studies of galaxy formation (e.g., Peng et al. 2010; Behroozi et al. 2013; Lilly et al. 2013). Alternatively, our AGN variability prescriptions could be incorporated into semi-analytic models of galaxy formation based on dark matter halo merger trees, which explicitly track the stellar and BH masses and SFRs of each component galaxy (e.g., Bower et al. 2006; Somerville et al. 2008; Fanidakis et al. 2012, 2013). By comparing these more sophisticated models to observations, we may be able to obtain a reliable picture of the variability of AGNs and the connection between BH accretion and SF.

As discussed in Section 1, a complete understanding of AGN variability may potentially reconcile a range of seemingly contradictory observations about the relationships between AGNs and their host galaxies. However, the stochastic nature of the variability also requires that we employ an inherently statistical approach in observational studies by measuring the *distribution* in AGN accretion rates as a function of galaxy properties. Currently, X-ray surveys provide one of the most robust methods for probing AGN accretion over a wide range of Eddington ratios, host galaxy properties, and redshifts (e.g., Hopkins et al. 2009), and have enabled the first such statistical studies at moderate to high redshift (e.g., Hickox et al. 2009; Aird et al. 2012; Bongiorno et al. 2012). Using these techniques and existing X-ray and far-IR observations, it might be possible to obtain a measurement of the distribution of $L_{\rm AGN}$ in broad bins of SFR, which would provide an interesting constraint on our model's prediction[6] that the distribution in $L_{\rm AGN}/{\rm SFR}$ is independent of SFR or redshift. An alternative could be to measure the distribution of $L_{\rm IR}$ in bins of $L_{\rm AGN}$, for which the model also makes clear predictions as shown in Figure 4. However, to explore the distribution of AGN accretion rate as a function of several interesting host galaxy properties (i.e., SFR, stellar mass, redshift) would require larger X-ray AGN samples than are currently available. Our results therefore provide motivation for future deep, wide extragalactic surveys that will obtain large samples of AGNs over a wide range in redshift and luminosity.

[6] Data and software for computing the predictions of the model at a given redshift and $L_{\rm AGN}$ or $L_{\rm IR}$ are available at http://www.dartmouth.edu/~hickox/sfagn.php.

We thank David Rosario, Sara Ellison, and Philip Hopkins for helpful discussions, and are grateful to the anonymous referee for constructive comments that improved the paper. J.R.M. and D.M.A. acknowledge generous support from the Leverhulme Trust. F.C. acknowledges support by the NASA contract 11-ADAP11-0218. C.-T.J.C. acknowledges support from a Dartmouth Fellowship. This work was supported in part by Chandra grant SP8-9001X. This research has made use of NASA's Astrophysics Data System.

REFERENCES

Aird, J., Coil, A. L., Moustakas, J., et al. 2012, ApJ, 746, 90
Aird, J., Coil, A. L., Moustakas, J., et al. 2013, ApJ, 775, 41
Aird, J., Nandra, K., Laird, E. S., et al. 2010, MNRAS, 401, 2531
Alexander, D. M., & Hickox, R. C. 2012, NewAR, 56, 93
Allevato, V., Finoguenov, A., Cappelluti, N., et al. 2011, ApJ, 736, 99
Anglés-Alcázar, D., Özel, F., & Davé, R. 2013a, ApJ, 770, 5
Anglés-Alcázar, D., Özel, F., Davé, R., et al. 2013b, ApJ, submitted (arXiv:1309.5963)
Behroozi, P. S., Wechsler, R. H., & Conroy, C. 2013, ApJ, 770, 57
Bonfield, D. G., Jarvis, M. J., Hardcastle, M. J., et al. 2011, MNRAS, 416, 13
Bongiorno, A., Merloni, A., Brusa, M., et al. 2012, MNRAS, 427, 3103
Bower, R. G., Benson, A. J., Malbon, R., et al. 2006, MNRAS, 370, 645
Boyle, B. J., & Terlevich, R. J. 1998, MNRAS, 293, L49
Capelli, R., Warwick, R. S., Porquet, D., Gillessen, S., & Predehl, P. 2012, A&A, 545, A35
Cappelluti, N., Allevato, V., & Finoguenov, A. 2012, AdAst, 2012, 853701
Cardamone, C. N., Urry, C. M., Schawinski, K., et al. 2010, ApJL, 721, L38
Chabrier, G. 2003, PASP, 115, 763
Chary, R., & Elbaz, D. 2001, ApJ, 556, 562
Chen, C.-T. J., Hickox, R. C., Alberts, S., et al. 2013, ApJ, 773, 3
Chen, W., Shrader, C. R., & Livio, M. 1997, ApJ, 491, 312
Ciotti, L., Ostriker, J. P., & Proga, D. 2010, ApJ, 717, 708
Cisternas, M., Jahnke, K., Inskip, K. J., et al. 2011, ApJ, 726, 57
Civano, F., Elvis, M., Brusa, M., et al. 2012, ApJS, 201, 30
Coil, A. L., Georgakakis, A., Newman, J. A., et al. 2009, ApJ, 701, 1484
Colbert, J. W., Teplitz, H. I., Yan, L., Malkan, M. A., & McCarthy, P. J. 2005, ApJ, 621, 587
Conroy, C., & White, M. 2013, ApJ, 762, 70
Cusumano, G., La Parola, V., Segreto, A., et al. 2010, A&A, 524, A64
Diamond-Stanic, A. M., & Rieke, G. H. 2012, ApJ, 746, 168
Di Matteo, T., Springel, V., & Hernquist, L. 2005, Natur, 433, 604
Donoso, E., Li, C., Kauffmann, G., Best, P. N., & Heckman, T. M. 2010, MNRAS, 407, 1078
Draper, A. R., & Ballantyne, D. R. 2012, ApJ, 751, 72
Elbaz, D., Dickinson, M., Hwang, H. S., et al. 2011, A&A, 533, A119
Ellison, S. L., Mendel, J. T., Scudder, J. M., Patton, D. R., & Palmer, M. J. D. 2013, MNRAS, 430, 3128
Ellison, S. L., Patton, D. R., Mendel, J. T., & Scudder, J. M. 2011, MNRAS, 418, 2043
Esquej, P., Alonso-Herrero, A., González-Martín, O., et al. 2014, ApJ, 780, 86
Fanidakis, N., Baugh, C. M., Benson, A. J., et al. 2012, MNRAS, 419, 2797
Fanidakis, N., Georgakakis, A., Mountrichas, G., et al. 2013, MNRAS, 435, 679
Ferrarese, L., & Merritt, D. 2000, ApJL, 539, L9
Gabor, J. M., & Bournaud, F. 2013, MNRAS, 434, 606
Gebhardt, K., Bender, R., Bower, G., et al. 2000, ApJL, 539, L13
Georgakakis, A., Nandra, K., Yan, R., et al. 2008, MNRAS, 385, 2049
Ghez, A. M., Salim, S., Weinberg, N. N., et al. 2008, ApJ, 689, 1044
Gillessen, S., Eisenhauer, F., Trippe, S., et al. 2009, ApJ, 692, 1075
Gonçalves, T. S., Steidel, C. C., & Pettini, M. 2008, ApJ, 676, 816
Goulding, A. D., Forman, W. R., Hickox, R. C., et al. 2013, ApJ, submitted (arXiv:1310.8298)
Gruppioni, C., Pozzi, F., Rodighiero, G., et al. 2013, MNRAS, 432, 23
Gültekin, K., Richstone, D. O., Gebhardt, K., et al. 2009, ApJ, 698, 198
Haggard, D., Green, P. J., Anderson, S. F., et al. 2010, ApJ, 723, 1447
Hainline, K. N., Shapley, A. E., Greene, J. E., et al. 2012, ApJ, 760, 74
Harrison, C. M., Alexander, D. M., Mullaney, J. R., et al. 2012, ApJL, 760, L15
Hickox, R. C., Jones, C., Forman, W. R., et al. 2009, ApJ, 696, 891
Hickox, R. C., Myers, A. D., Brodwin, M., et al. 2011, ApJ, 731, 117
Hickox, R. C., Wardlow, J. L., Smail, I., et al. 2012, MNRAS, 421, 284

Hicks, E. K. S., Davies, R. I., Maciejewski, W., et al. 2013, ApJ, 768, 107
Hopkins, P. F., & Hernquist, L. 2009, ApJ, 698, 1550
Hopkins, P. F., Hernquist, L., Cox, T. J., et al. 2005, ApJ, 630, 716
Hopkins, P. F., Hickox, R., Quataert, E., & Hernquist, L. 2009, MNRAS, 398, 333
Hopkins, P. F., & Quataert, E. 2010, MNRAS, 407, 1529
Hopkins, P. F., Richards, G. T., & Hernquist, L. 2007, ApJ, 654, 731
Hopkins, P. F., Somerville, R. S., Hernquist, L., et al. 2006, ApJ, 652, 864
Hopkins, P. F., Younger, J. D., Hayward, C. C., Narayanan, D., & Hernquist, L. 2010, MNRAS, 402, 1693
Hung, C.-L., Sanders, D. B., Casey, C. M., et al. 2013, ApJ, 778, 129
Jakobsen, P., Jansen, R. A., Wagner, S., & Reimers, D. 2003, A&A, 397, 891
Juneau, S., Dickinson, M., Bournaud, F., et al. 2013, ApJ, 764, 176
Kartaltepe, J. S., Dickinson, M., Alexander, D. M., et al. 2012, ApJ, 757, 23
Kartaltepe, J. S., Sanders, D. B., Le Floc'h, E., et al. 2010, ApJ, 721, 98
Kauffmann, G., & Heckman, T. M. 2009, MNRAS, 397, 135
Kauffmann, G., Heckman, T. M., Tremonti, C., et al. 2003, MNRAS, 346, 1055
Keel, W. C., Chojnowski, S. D., Bennert, V. N., et al. 2012a, MNRAS, 420, 878
Keel, W. C., Lintott, C. J., Schawinski, K., et al. 2012b, AJ, 144, 66
Kelly, B. C., & Shen, Y. 2013, ApJ, 764, 45
Kelly, B. C., Vestergaard, M., Fan, X., et al. 2010, ApJ, 719, 1315
Kennicutt, R. C., Jr. 1998, ARA&A, 36, 189
Kirkman, D., & Tytler, D. 2008, MNRAS, 391, 1457
Kirkpatrick, A., Pope, A., Charmandaris, V., et al. 2013, ApJ, 763, 123
Kocevski, D. D., Faber, S. M., Mozena, M., et al. 2012, ApJ, 744, 148
Koss, M., Mushotzky, R., Veilleux, S., & Winter, L. 2010, ApJL, 716, L125
LaMassa, S. M., Heckman, T. M., Ptak, A., & Urry, C. M. 2013, ApJL, 765, L33
Li, C., Kauffmann, G., Wang, L., et al. 2006, MNRAS, 373, 457
Lilly, S. J., Carollo, C. M., Pipino, A., Renzini, A., & Peng, Y. 2013, ApJ, 772, 119
Lintott, C. J., Schawinski, K., Keel, W., et al. 2009, MNRAS, 399, 129
Lutz, D., Mainieri, V., Rafferty, D., et al. 2010, ApJ, 712, 1287
Lutz, D., Sturm, E., Tacconi, L. J., et al. 2008, ApJ, 684, 853
Magorrian, J., Tremaine, S., Richstone, D., et al. 1998, AJ, 115, 2285
McHardy, I. M. 2013, MNRAS, 430, L49
McNamara, B. R., & Nulsen, P. E. J. 2007, ARA&A, 45, 117
Melbourne, J., Koo, D. C., & Le Floc'h, E. 2005, ApJL, 632, L65
Merloni, A., & Heinz, S. 2008, MNRAS, 388, 1011
Merloni, A., & Heinz, S. 2013, in Planets, Stars and Stellar Systems, ed. T. D. Oswalt & W. C. Keel (Vol. 6; Dordrecht: Springer), 503
Mullaney, J. R., Alexander, D. M., Goulding, A. D., & Hickox, R. C. 2011, MNRAS, 414, 1082
Mullaney, J. R., Daddi, E., Béthermin, M., et al. 2012a, ApJL, 753, L30
Mullaney, J. R., Pannella, M., Daddi, E., et al. 2012b, MNRAS, 419, 95
Nandra, K., Georgakakis, A., Willmer, C. N. A., et al. 2007, ApJL, 660, L11
Nayakshin, S. 2014, MNRAS, 418, 2404
Nayakshin, S., & Zubovas, K. 2012, MNRAS, 427, 372
Neistein, E., & Netzer, H. 2014, MNRAS, 437, 3373
Netzer, H. 2009, MNRAS, 399, 1907
Netzer, H., Lutz, D., Schweitzer, M., et al. 2007, ApJ, 666, 806
Nobuta, K., Akiyama, M., Ueda, Y., et al. 2012, ApJ, 761, 143
Noeske, K. G., Weiner, B. J., Faber, S. M., et al. 2007, ApJL, 660, L43
Novak, G. S., Ostriker, J. P., & Ciotti, L. 2011, ApJ, 737, 26
Peng, Y.-j., Lilly, S. J., Kovač, K., et al. 2010, ApJ, 721, 193
Ponti, G., Terrier, R., Goldwurm, A., Belanger, G., & Trap, G. 2010, ApJ, 714, 732
Rafferty, D. A., Brandt, W. N., Alexander, D. M., et al. 2011, ApJ, 742, 3
Remillard, R. A., & McClintock, J. E. 2006, ARA&A, 44, 49
Robitaille, T. P., & Whitney, B. A. 2010, ApJL, 710, L11
Rosario, D. J., Mozena, M., Wuyts, S., et al. 2013a, ApJ, 763, 59
Rosario, D. J., Santini, P., Lutz, D., et al. 2012, A&A, 545, A45
Rosario, D. J., Santini, P., Lutz, D., et al. 2013b, ApJ, 771, 63
Ryu, S. G., Nobukawa, M., Nakashima, S., et al. 2013, PASJ, 65, 33
Sabater, J., Best, P. N., & Argudo-Fernández, M. 2013, MNRAS, 430, 638
Santini, P., Rosario, D. J., Shao, L., et al. 2012, A&A, 540, A109
Sarzi, M., Shields, J. C., Schawinski, K., et al. 2010, MNRAS, 402, 2187
Schawinski, K., Evans, D. A., Virani, S., et al. 2010, ApJL, 724, L30
Schawinski, K., Simmons, B. D., Urry, C. M., Treister, E., & Glikman, E. 2012, MNRAS, 425, L61
Schawinski, K., Treister, E., Urry, C. M., et al. 2011, ApJL, 727, L31
Schirmer, M., Diaz, R., Holhjem, K., Levenson, N. A., & Winge, C. 2013, ApJ, 763, 60
Shankar, F., Weinberg, D. H., & Miralda-Escudé, J. 2013, MNRAS, 428, 421
Shao, L., Lutz, D., Nordon, R., et al. 2010, A&A, 518, L26
Shen, Y., & Kelly, B. C. 2012, ApJ, 746, 169
Shi, Y., Rieke, G., Lotz, J., & Perez-Gonzalez, P. G. 2009, ApJ, 697, 1764
Siemiginowska, A., Czerny, B., Janiuk, A., et al. 2010, in ASP Conf. Ser. 427, Accretion and Ejection in AGN: A Global View, ed. L. Maraschi, G. Ghisellini, R. Della Ceca, & F. Tavecchio (San Francisco, CA: ASP), 326
Siemiginowska, A., & Elvis, M. 1997, ApJL, 482, L9
Silverman, J. D., Green, P. J., Barkhouse, W. A., et al. 2008, ApJ, 679, 118
Silverman, J. D., Lamareille, F., Maier, C., et al. 2009, ApJ, 696, 396
Singh, R., van de Ven, G., Jahnke, K., et al. 2013, A&A, 558, A43
Somerville, R. S., Hopkins, P. F., Cox, T. J., Robertson, B. E., & Hernquist, L. 2008, MNRAS, 391, 481
Starikova, S., Cool, R., Eisenstein, D., et al. 2011, ApJ, 741, 15
Su, M., & Finkbeiner, D. P. 2012, ApJ, 753, 61
Symeonidis, M., Georgakakis, A., Seymour, N., et al. 2011, MNRAS, 417, 2239
Symeonidis, M., Kartaltepe, J., Salvato, M., et al. 2013, MNRAS, 433, 1015
Treister, E., Schawinski, K., Urry, C. M., & Simmons, B. D. 2012, ApJL, 758, L39
Ulrich, M.-H., Maraschi, L., & Urry, C. M. 1997, ARA&A, 35, 445
Urrutia, T., Lacy, M., & Becker, R. H. 2008, ApJ, 674, 80
Wang, J. L., Xia, X. Y., Mao, S., et al. 2006, ApJ, 649, 722
Xue, Y. Q., Brandt, W. N., Luo, B., et al. 2010, ApJ, 720, 368
Yan, R., & Blanton, M. R. 2012, ApJ, 747, 61
Zubovas, K., King, A. R., & Nayakshin, S. 2011, MNRAS, 415, L21
Zubovas, K., & Nayakshin, S. 2012, MNRAS, 424, 666
Zubovas, K., Nayakshin, S., King, A., & Wilkinson, M. 2013, MNRAS, 433, 3079